PCIM Europe 2022; International Exhibition and Conference for Power Electronics, Intelligent Motion, Renewable Energy and Energy Management; Proceedings of

Flexible Operation of Variable Speed Direct-MMC in Hydropower Applications

P. Bontemps and D. Dujic

POWER ELECTRONICS LABORATORY
ÉCOLE POLYTECHNIQUE FÉDÉRALE DE LAUSANNE

 DOI:10.30420/565822034

Flexible Operation of Variable Speed Direct-MMC in Hydropower Applications

Philippe Bontemps, Drazen Dujic

École Polytechnique Fédérale de Lausanne (EPFL), Power Electronics Laboratory, Switzerland

Corresponding author: Philippe Bontemps, philippe.bontemps@epfl.ch

Abstract

This paper presents a flexible and grid code complying operation of the matrix modular multilevel converter used in a variable speed drive pumped hydro storage power plants. A hardware-in-the-loop platform, where the control algorithm is deployed on the ABB PEC800 controller, is described and used to explore and create high fidelity results for the considered scenarios. The inaccessibility of converters fulfilling typical pumped hydro storage power plant ratings, require a thorough verification process through simulations, lowering the risks of potential damages to the high value equipment. The hardware-in-the-loop platform provides very accurate and very low risk simulation method and is used in this paper to demonstrate the achieved increase in flexibility of the pumped hydro storage power plant. Compliance with the grid code is demonstrated through simulations involving frequency deviations and voltage sags, which are included in the paper. Additionally, a detailed description of the control algorithm deployed on the hardware-in-the-loop achieving grid compliance and energy control of the matrix modular multilevel converter is provided.

1 Introduction

To remain competitive on the energy market and cope with the increasing installed capacity of intermittent renewable energies, Pumped Hydro Storage Power Plant (PHSP) need to migrate to variable speed, allowing to track fast varying power references, fast speed reversal transients as well as to offer increased efficiency [1]–[3]. A power electronics converter is required to achieve variable speed operation, but the high power requirements of PHSP constitute a challenge for Variable Speed Drive (VSD) technology, making conventional converter topologies and standard ratings unsuited for such applications.

Two main VSD configuration can be distinguished, namely the Doubly Fed Induction Machine (DFIM) shown in Fig. 1a and the Converter Fed Synchronous Machine (CFSM) shown in Fig. 1b. The main advantage of the DFIM configuration, responsible for its popularity for power levels exceeding 100 MW, is the reduced converter power ratings processing only the slip power which consists of typically around 30% of the pumping power and achieves a $\pm$10% speed variation. The technological feasibility and commercial availability of converters fulfilling the power ratings of a DFIM configuration are the reason for its popularity among VSD PHSPs. While there are many DFIM installations worldwide, there are also several drawbacks of this configuration such as the increased complexity of the rotor design, limited starting torque requiring dewatering of the chamber and the limited low voltage ride-through capabilities.

Unlike the DFIM configuration, the CFSM requires the converter to be rated to the same power of the PHSP, as connected directly to the stator it processes the full stator power of the machine. The

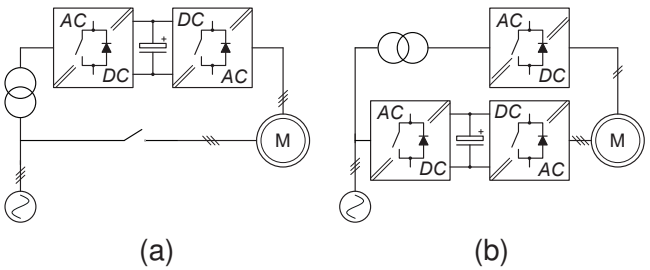

Fig. 1: Simplified representation of two typical variable speed drive configurations used in PHSP, (a) DFIM and (b) CFSM.

ISBN 978-3-8007-5822-7

increased power rating of the converter eliminates the aforementioned drawbacks of the DFIM configuration, however, the challenge with the CFSM lies in achieving the required converter power ratings. For units around 100 MW only two CFSM configurations exist, namely the Grimsel 2 power plant in Switzerland and the Galgenbichl power plant in Austria [4], [5]. The former retrofitted one out of its four 90 MW Synchronous Machine (SM) with a full size power electronics converter, and the latter one is a new installation with two 80 MW machines in a CFSM configuration.

The rise of the Modular Multilevel Converter (MMC) technology, relying on the series connection of cells, allows the power and voltage to be scaled to the requirements of PHSP. This advantage over conventional monolithic multilevel converters, leads to the feasibility of high power CFSM installations [6]–[8]. Current scaling of the MMC topology can be achieved by parallel connection of either cells, branches, subclusters or converters [9].

Within the family of MMC, the Matrix Modular Multilevel Converter (M3C), being optimized for low frequency high power drives, is especially suited for the transition to variable speed in PHSP [10]. Figure 2 shows the M3C interfacing the electrical machine of a PHSP and the ac grid using nine branches connecting each of the three input phases to the three output phases. The M3C allows for a transformer-less connection to the grid provided that the voltage of the SM matches the voltage of the ac grid. As a branch must realize both positive and negative voltages, it consists of a series connection of Full Bridge (FB) cells, even though different cell topologies are possible [11]. One major operational limitation is the low frequency branch energy oscillation in case the load frequency approaches the grid frequency. For this reason, the M3C topology is designed for applications with different frequencies at the two ac terminals.

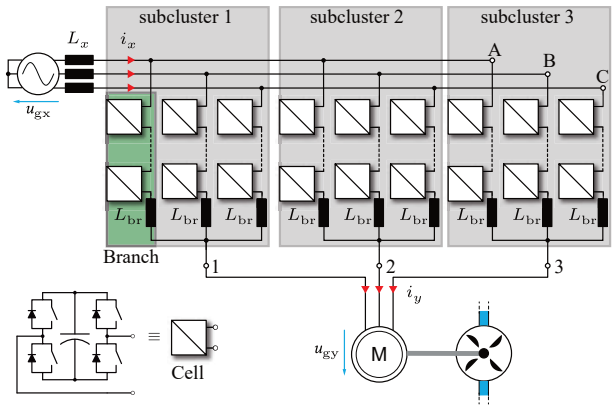

Fig. 2: The matrix modular multilevel converter with the three subclusters, highlighted in gray, each containing three branches, highlighted in green, and N cells per branch. The two AC systems are represented by a grid and a 3 phase machine connected to a pump/turbine.

Due to the high number of distributed capacitances, the control of the M3C aiming to fulfill machine and grid side power requirements while balancing the energy between the cells is a major challenge. Hardware-In-The-Loop (HIL) testing prior to the deployment in the field allows for a thorough verification of control structure and algorithm without risk of damaging high value equipment.

The structure of the paper is the following: section 2 introduces the HIL platform on which the control algorithm is implemented and which is used to collect the results shown in this paper. Section 3 describes the control algorithm that is implemented on the HIL, including a description of the grid current control, machine side vector control and the internal M3C energy control to keep the branch energies balanced. Section 4 shows the simulation results and the performance of the M3C regarding grid code compliance and flexible operation of the PHSP, and Section 5 concludes the paper.

2 Hardware-in-the-loop setup

Figure 3 shows the HIL platform developed at the Power Electronics Laboratory at EPFL using a connection of multiple small scale simulators (RT Box). A total of nine branch RT Boxes, simulating the nine branches of the M3C and one application RT Box, hosting the grid and machine models and mapping the signals from the branch RT Box, are used to simulate the M3C. Each of the nine branch RT Boxes hosting the power stage of the cells is connected through an interface board to eight cell card hosting the logical circuit.

The control is deployed on ABB PEC800 controllers which are connected at the back of the cabinet shown in Fig. 3. The cell cards receive voltage and current references through Fiber Optical Link (FOL) from the controller and based on the relevant measurements generate switching signals that are sent to the Branch RT Box.

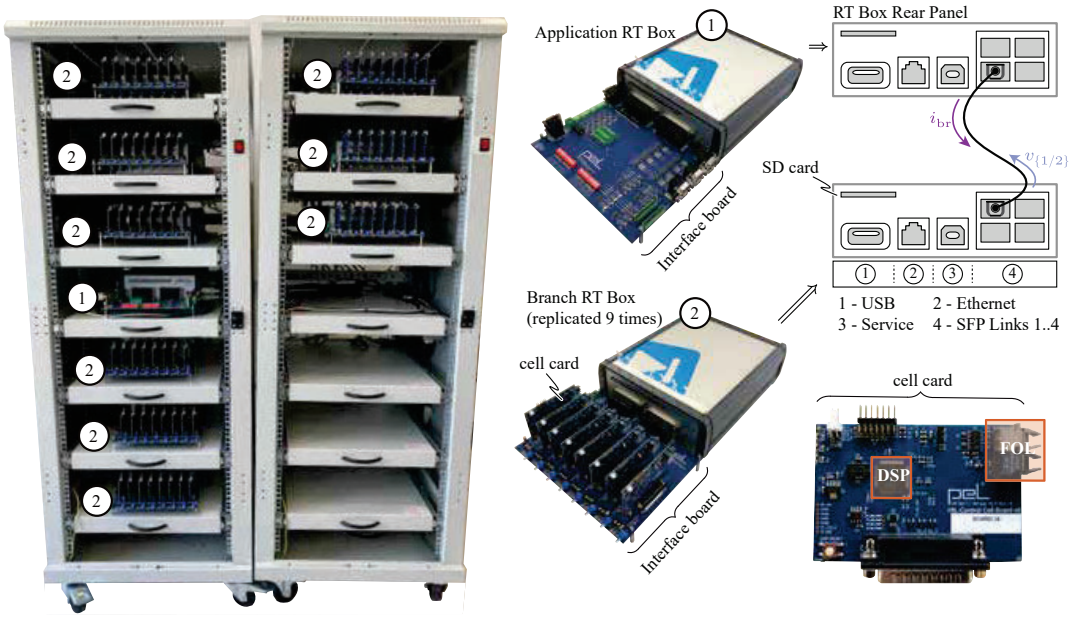

Fig. 3: HIL system used for M3C control structure and algorithm verification purpose. The left side shows a front picture of the HIL and a zoomed picture of both the application and Branch RT Box is shown in the middle labeled by 1 and 2 with their interconnection shown on the top right. The logical circuit of the cells is implemented on the cell card shown on the bottom right. The back side of the cabinet hosts the ABB PEC800, not visible in the figure

A detailed description of the M3C model running on the HIL including a validation of the obtained simulation results can be found in [12].

3 Control algorithm

Implemented on ABB PEC800 controllers, the control algorithm of the M3C guarantees balancing of the M3C energy, while ensuring on one side the proper operation of the connected SM and respecting the grid code on the other side. The modulation method used on the M3C is the Phase Shifted Carrier (PSC) modulation, and each cell receives its voltage reference from the ABB PEC800.

For the grid current control, a FLL provides estimation of the grid frequency and extracts positive and negative sequence of the grid voltages. Using the Instantaneous Active and Reactive Control (IARC), and a PR controller with resonance at the grid frequency, the voltage reference for the grid side terminals are generated.

The generation of the voltage references for the electrical machine terminals of the M3C is achieved using a classical vector control scheme.

3.1 Grid control

The grid terminal voltage of the M3C has to comply with the grid code requirements. In the case of this paper, the German grid code is taken as a reference [13]. The control method chosen in this paper is the IARC, as introduced in [14].

To allow a power exchange with the grid even under faulty grid conditions, both positive and negative sequence voltage have to be extracted from the measured grid voltages. The usage of a stationary reference frame allows the implementation of the Decoupled Second Order General Integrator (DSOGI) with Frequency Lock Loop (FLL) as shown in Fig. 4 (a). Depending on the amplitude of the measured positive sequence grid voltage, the grid code requires the injection or absorption of reactive power, implemented as shown in Fig. 4 (b). Taking into account the required reactive power reference and the maximum available apparent power, the maximum possible active power reference can be computed. Following these power reference calculations, the required grid current references can be computed in $\alpha\beta$-frame as shown in Fig. 4 (c). Finally the grid voltage reference is obtained using a PR controller shown in Fig. 4 (d).

The German grid code requirements which define

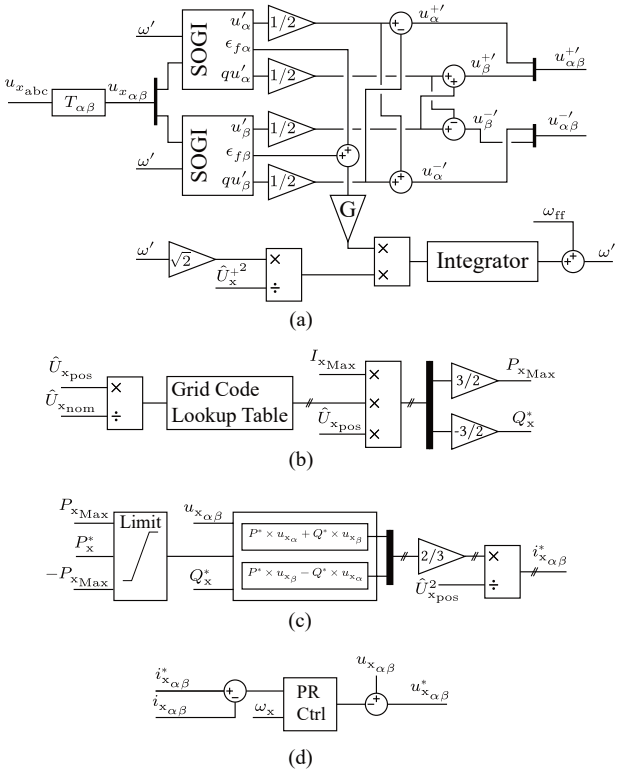

Fig. 4: Grid current control implementation. (a) shows the implementation of the FLL to extract both positive and negative sequence as well as the frequency of the grid voltages. (b) shows the implementation of the active and reactive power reference. (c) shows the computation of the grid current references which are used in the PR controller shown in (d).

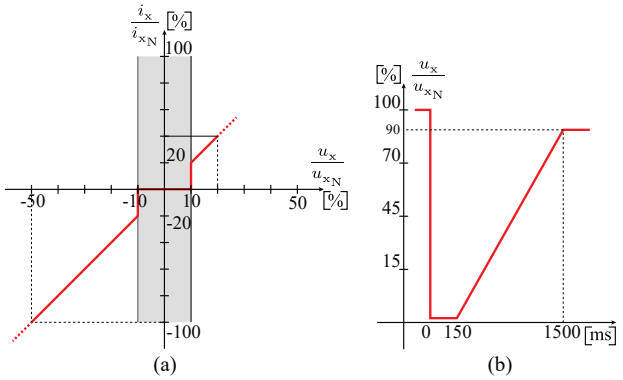

Fig. 5: Grid scenarios as defined by the German grid code. (a) shows the amount of reactive current to inject into or absorb from the grid depending on the voltage sag or rise. (b) shows the limit of a voltage sag above which the converter must remain connected to the grid and provide reactive power.

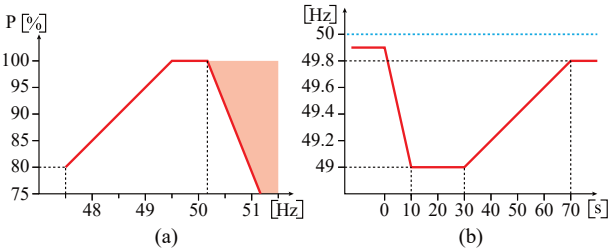

Fig. 6: Grid scenarios as defined by the German grid code. (a) shows the minimum amount of active power generation depending on the grid frequency. (b) shows the limit of a frequency deviation above which the converter must provide the nominal power to the grid.

the amount of reactive power to inject to or absorb from the grid is shown in Fig. 5 (a). A grid voltage amplitude variation lower than ±10% of the nominal voltage does not require any reactive power reference from the converter, and beyond that limit the reactive power reference is defined by the red line. Figure 5 (b) shows the maximum Low Voltage Ride Through (LVRT) defined by the German grid code throughout which the converter must provide the required amount of reactive power to the grid. For any voltage variation beyond the line of Fig. 5 (b), the converter is allowed to disconnect from the grid.

Figure 6 shows the German grid code requirements regarding active power generation during grid frequency deviations. If the grid frequency varies lower than 49.5 Hz, the minimum required active power generation is defined by the red line in Fig. 6 (a), whereas for a frequency lower than 47.5 Hz, the converter is allowed to disconnect from the grid. Exceeding the value of 50.2 Hz, the active power injection to the grid must be limited to a maximum defined by the red line in Fig. 6 (a). The worst scenario during which the full nominal power must be injected to the grid is shown in Fig. 6 (b). Any frequency deviation exceeding the red line allows a reduction in active power generation defined by Fig. 6 (a).

While this paper uses the German grid code, similar grid codes are available in different countries, with small differences.

3.2 Synchronous machine control

Figure 7 shows the implementation of the classical and well established vector control used for the SM. The depicted control used during operation of the M3C in power mode is shown in Fig. 7 (b). In this operation mode, the speed of the SM is defined by

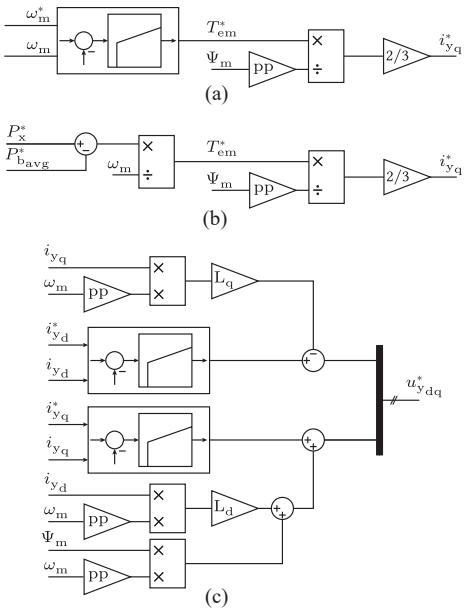

Fig. 7: Synchronous machine current control implementation. (a) showing the q-current reference calculation using the speed controller. (b) showing the q-current reference calculation using the power reference. (c) showing the vector control implementation

the load torque and the power reference imposed by the grid operator to which the losses in the M3C are added. During some transients such as speed up or speed reversal of the SM, the speed control showed in Fig. 7 (a) is used. In this case the active power absorbed or injected into the grid is defined by the total energy controller, keeping the overall energy in the M3C constant. The implementation of the vector control scheme is shown in Fig. 7 (c).

3.3 Branch balancing control

With the grid current control and the machine vector control, the terminal currents of the M3C are controlled to fulfill both grid and machine requirements. Doing so creates a branch current containing both input and output frequencies. For a current flowing in the branch connecting the input phase x to the output phase y the expression is:

$$i_{\mathrm{xy}}(t) = \frac{1}{3}\left(i_{\mathrm{x}}(t) + i_{\mathrm{y}}(t)\right) \tag{1}$$

$$i_{\mathrm{xy}}(t) = \frac{1}{3}\left(\hat{I}_{\mathrm{x}}\sin\left(\omega_x t + \phi_{\mathrm{x}}\right) + \hat{I}_{\mathrm{y}}\sin\left(\omega_y t + \phi_{\mathrm{y}}\right)\right) \tag{2}$$

However, to assure proper operation of the M3C, the average energy in all nine branches must be

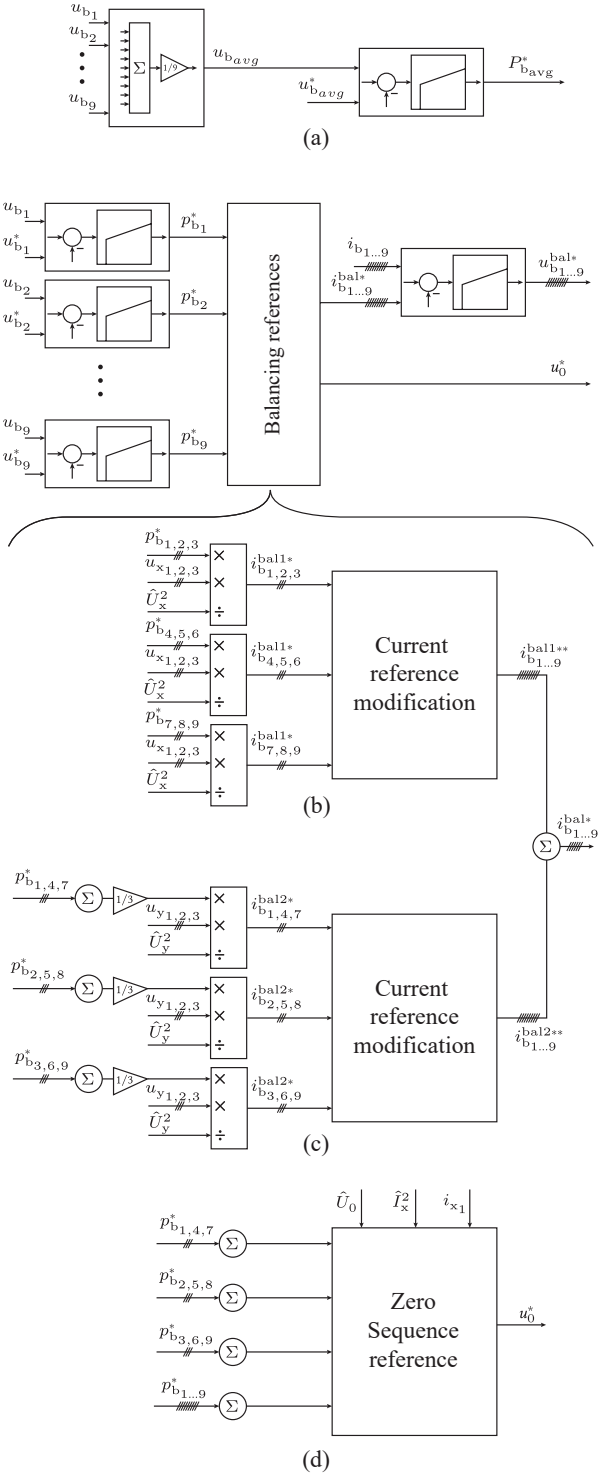

Fig. 8: Structure of the direct branch energy balancing method. (a) shows the total energy control part, keeping the overall energy in the branches constant. (b) shows the reference calculation of the circulating currents acting on the grid voltage. (c) shows the circulating current reference calculation acting on the load voltages. (d) shows the common mode voltage calculation used when no load voltage are available.

equal, leading to the necessity of an additional control layer, ensuring equal energy distribution among the branches. This energy balancing control of the M3C can be separated in two major categories. The first category is the balancing between the branches of the same subcluster (shown in Fig. 2), meaning the branches that are connected to the same output phase. The second category of balancing is between branches of different subclusters and connected to the same input phase. While these two balancing actions must be achieved, the resulting balancing current must neither influence the input or the output terminal currents. Additionally to these two categories, a total energy controller, regulating the input and output power to cancel each other out, thus ensuring constant average energy in the M3C has to be added.

The total energy control of the M3C, as shown in Fig. 8 (a), is done using the average of all nine branches voltages to which the reference branch voltage is subtracted and using a PI controller, the needed power reference can be computed.

To achieve balancing between the branches, each branch voltage is converted to the respective branch energy and compared to its reference, and using a PI controller, the required power reference to achieve balancing for the given branch is computed. However, these power references have to be modified before being transmitted to the branches as to make sure that the resulting circulating current does not influence neither the input nor the output terminal currents. In order to create the given circulating power references, corresponding circulating currents acting on present branch voltages are to be calculated. During operation of the SM, branch voltages consist of the input and output terminal voltages, however, in case no output voltage is present, another degree of freedom, namely the common mode voltage has to be used.

During normal operation, the balancing of the energy between the branches is achieved through circulating current acting on the input voltages, shown in Fig. 8 (b), and the output voltages, shown in Fig. 8 (c). To make sure that these circulating currents influence neither of the terminal currents, the modification of the circulating current references as presented in [15] is used. In case of missing load voltages, Fig. 8 (c) is replaced by (d) which is generating a common mode voltage acting on the input currents to allow balancing of the energy between the branches.

Tab. 1: Details of the grid, SM and M3C model running on HIL. The ratings of the SM are scaled values from the PHSP test rig present at the Power Electronics Laboratory at EPFL.

	Value	Unit
Grid Voltage	6	kV
SM Voltage	6.6	kV
SM Power	500	kVA
SM Torque	6088	Nm
SM Speed	750	rpm
Shaft inertia	152	kgm^2
M3C cell capacitance	1	mF
M3C cell voltage	1500	V
M3C branch inductance	2.5	mH
M3C branch resistance	66.4	mΩ

The final branch voltage references are:

$$u^*_{\mathrm{b}_{1\ldots3}} = u^*_{\mathrm{x}_{1\ldots3}} - u^*_{\mathrm{y}_1} + u^{\mathrm{bal}*}_{\mathrm{b}_{1\ldots3}} - u^*_0 \tag{3}$$

$$u^*_{\mathrm{b}_{4\ldots6}} = u^*_{\mathrm{x}_{1\ldots3}} - u^*_{\mathrm{y}_2} + u^{\mathrm{bal}*}_{\mathrm{b}_{4\ldots6}} - u^*_0 \tag{4}$$

$$u^*_{\mathrm{b}_{7\ldots9}} = u^*_{\mathrm{x}_{1\ldots3}} - u^*_{\mathrm{y}_3} + u^{\mathrm{bal}*}_{\mathrm{b}_{7\ldots9}} - u^*_0 \tag{5}$$

4 Simulation results

Three scenarios, namely a power reference change as well as two fault scenarios including a LVRT and a frequency deviation are run on the HIL. The details of the simulation model running on the HIL are presented in Tab. 1.

4.1 Power reference change

Figure 9 shows a power reference change in pumping mode, where in the first part, the power reference is dropped from 500 kW to 300 kW and in the second part the power reference is increased back to 500 kW. After the power reference drop, the speed of the SM drops from 750 rpm to 450 rpm at a rate defined by the load torque and the shaft inertia. The branch voltages, thus also the cell voltage, which represent the cell energy, remain constant throughout the process of power reference drop as shown by the branch voltage waveform at the bottom of the Fig. 9. The reduction in the amplitude of the branch voltage oscillations after the power reference change is explained by the reduced power flowing through the branches.

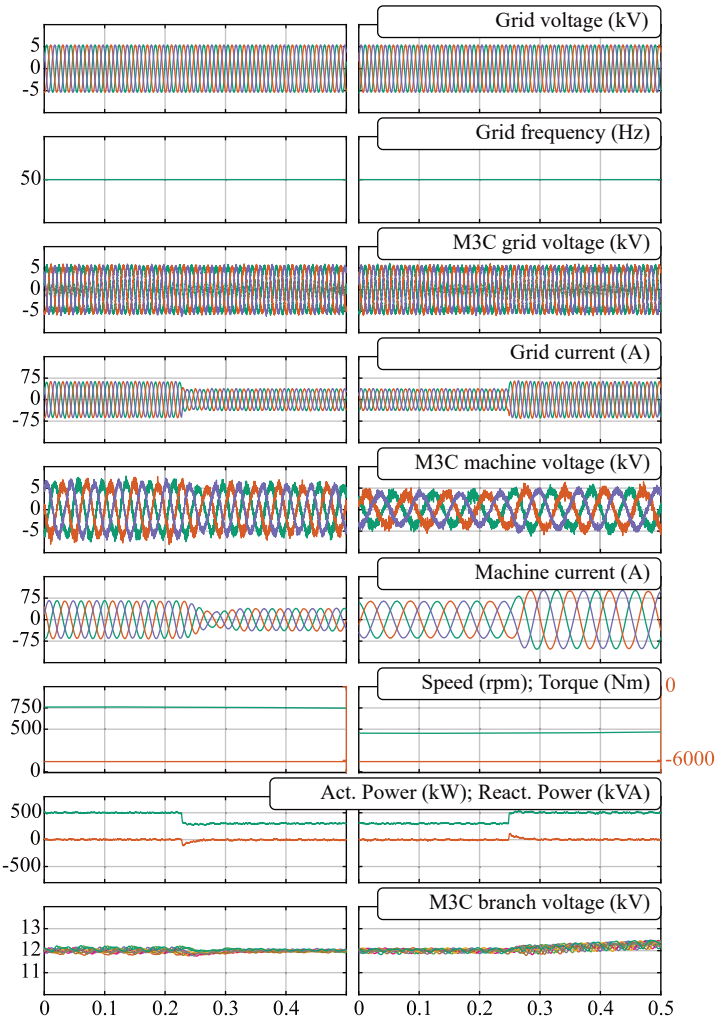

Fig. 9: Power reference change from 500 kW to 300 kW and back to 500 kW.

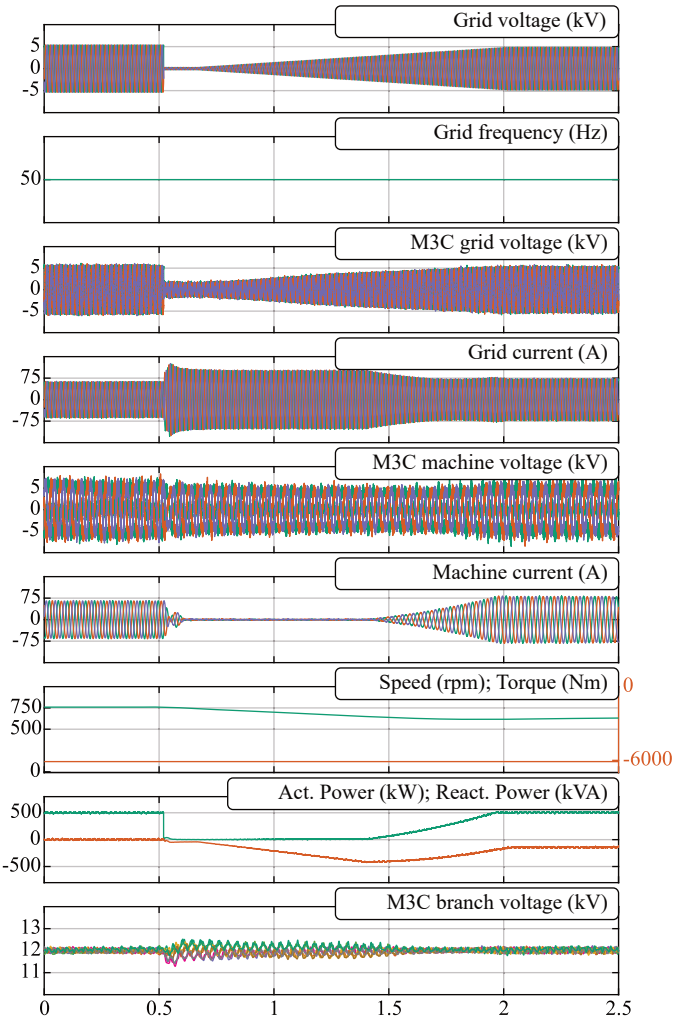

Fig. 10: Voltage sag following the profile as shown in Fig. 5 (b).

The right side of Fig. 9 shows the power reference rise from 300 kW to 500 kW which is achieved by exceeding the nominal stator current during the transient where the machine is accelerated back to its nominal speed. The excess of current is necessary as to achieve the correct power reference considering the lower induced stator voltage of the SM due to its reduced speed. As for the power reference drop, the energy balancing between the branches is achieved and shown on the lower part of Fig. 9.

4.2 Low voltage ride through

Figure 10 shows a voltage sag on the grid following the profile defined in the German grid code shown in Fig. 5 (b). After the voltage sag, maximum reactive current is injected into the grid, which in this case corresponds to 100 A and the active power is reduced to zero. During the grid voltage ramp up, the injected reactive current corresponds to the relation shown in Fig. 5 (a), and the active power reference is adapted as to operate the M3C at maximum power. As a consequence of the active power reference from the grid being zero, the machine stator currents instantly drop to zero as to keep the total energy in the M3C constant. Once the grid voltage is high enough to enable active power exchange, the SM current and in consequence also the SM speed are ramped up. Following the voltage ramp up defined in Fig. 5 (a), the final grid voltage value is fixed at 90% of the nominal voltage and at this operating point, the converter keeps injecting 20% of its maximum value as reactive power into the grid.

The balancing of the energy between the branches is achieved throughout the whole scenario, as seen by the branch voltages shown in the bottom graph of Fig. 10. During the LVRT, a slight increase in

branch voltage oscillation can be observed, which is explained by the very low grid voltage limiting the balancing action acting on the grid voltage as shown in Fig. 8 (b). Even with a limited energy balancing action, none of the nine branch voltages are exceeding the 10% margin of it's nominal value.

4.3 Grid frequency deviation

Figure 11 shows the grid code compliant behavior of the M3C regarding a frequency deviation. For this scenario, the PHSP is operated in generating mode, and the power reference following a frequency decrease should not drop below the red line defined in Fig. 6 (a). While the grid frequency remains above 47.5 Hz, the converter must remain connected to the grid. To demonstrate the increased capability of the M3C regarding grid compliance, the rate of change of the grid frequency is higher and drops lower than the one defined in Fig. 6 (b) while ensuring nominal power injection to the grid. In this case the frequency is changed from 50 Hz to 47.5 Hz within one second, where it remains for one second and is ramped up to 50 Hz with the same rate of change. During the whole process, the active power reference remains unchanged, delivering the full active power to the grid, thus exceeding the requirements of the German grid code.

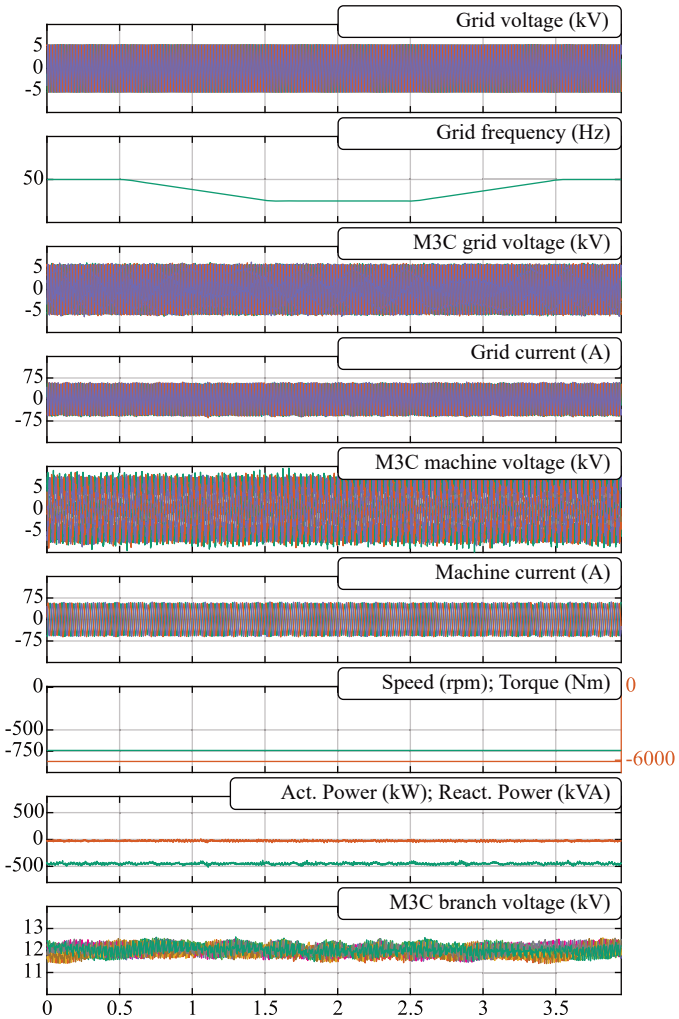

Fig. 11: Grid frequency deviation, following a faster rate of change than defined in Fig. 6 (b).

5 Conclusion

This paper presents the control structure of the M3C used for the simulation of a PHSP and demonstrates the gained flexibility through fast power reference changes in pumping mode as well as grid compliant behavior during grid faults such as LVRT and frequency deviations. As shown in the simulation results, the M3C exceeds grid code requirements during frequency deviations as it maintains nominal active power injection throughout a significantly more severe scenario than the one defined by the grid code. Balancing of the energy within the M3C without affecting terminal currents is achieved in all the simulation results using the direct-arm energy control presented above. The simulation presented in this paper are carried out on a HIL system explicitly developed to allow a thorough verification of the control structure and algorithm of the M3C without damaging high value equipment.

Acknowledgments

The results presented in this paper are supported in part by the European Union's Horizon 2020 research and innovation programme (Hydropower Extending Power System Flexibility (XFLEX HYDRO) project) under grant agreement No 857832 and in part by the Swiss Innovation Agency - Innosuisse under Innovation Project 38041.1 IP-ENG.

References

[1] A. Iwadachi, K. Tani, and K. Aguro, "The design of adjustable-speed pump-turbine modified from existing constant-speed on okutataragi power station," in *2016 19th International Conference on Electrical Machines and Systems (ICEMS)*, 2016, pp. 1–4.

[2] A. Vargas-Serrano, A. Hamann, S. Hedtke, C. M. Franck, and G. Hug, “Economic benefit analysis of retrofitting a fixed-speed pumped storage hydropower plant with an adjustable-speed machine,” in *2017 IEEE Manchester PowerTech*, 2017, pp. 1–6.

[3] P. Bontemps, N. Hugo, and D. Dujic, “Flexibility enhancements in pumped hydro storage power plants through variable speed drives,” in *IECON 2020 The 46th Annual Conference of the IEEE Industrial Electronics Society*, 2020, pp. 1820–1825.

[4] H. Schlunegger and A. Thöni, “100 MW full-size converter in the Grimsel 2 pumped-storage plant,” *Innsbruck, Hydro*, 2013.

[5] A. Christe, *Direct mmc for converter-fed synchronous machines*, https://www.epfl.ch/labs/pel/wp-content/uploads/2021/05/2021.05.11_IEEE_Webinar_Direct-MMC-Control_export.pdf [Accessed on 24.01.2022].

[6] P. K. Steimer, O. Senturk, S. Aubert, and S. Linder, “Converter-fed synchronous machine for pumped hydro storage plants,” in *2014 IEEE Energy Conversion Congress and Exposition (ECCE)*, 2014, pp. 4561–4567.

[7] M. Basić, A. Schwery, and D. Dujić, “Highly flexible indirect modular multilevel converter for high power pumped hydro storage plants,” in *IECON 2020 The 46th Annual Conference of the IEEE Industrial Electronics Society*, 2020, pp. 5290–5295.

[8] HITACHI ABB POWER GRIDS, *Flexible power for hydro pumped storage*, https://search.abb.com/library/Download.aspx?DocumentID=9AKK107992A6965&LanguageCode=en&DocumentPartId=&Action=Launch [Accessed on 24.01.2022].

[9] S. Milovanović and D. Dujić, “On facilitating the modular multilevel converter power scalability through branch paralleling,” in *2019 IEEE Energy Conversion Congress and Exposition (ECCE)*, 2019, pp. 6875–6882.

[10] M. Vasiladiotis, R. Baumann, C. Häderli, and J. Steinke, “Igct-based direct ac/ac modular multilevel converters for pumped hydro storage plants,” in *2018 IEEE Energy Conversion Congress and Exposition (ECCE)*, 2018, pp. 4837–4844.

[11] A. Nami, J. Liang, F. Dijkhuizen, and G. D. Demetriades, “Modular multilevel converters for hvdc applications: Review on converter cells and functionalities,” *IEEE Transactions on Power Electronics*, vol. 30, no. 1, pp. 18–36, 2015.

[12] P. Bontemps, S. Milovanovic, and D. Dujic, “Distributed real-time model of the m3c for hil systems using small-scale simulators,” *IEEE Open Journal of Power Electronics*, vol. 2, pp. 603–613, 2021.

[13] E.ON Netz GmbH and Verband Der Netzbetreiber Vnd, *Transmissioncode 2007. network and system rules of the german transmission system operators*, https://www.vde.com/resource/blob/937766/bfe325518ace878935966b6efbc493e4/transmissioncode-2007--network-and-system-rules-of-the-german-transmission-system-operators-data.pdf [Accessed on 24.01.2022].

[14] E. Watanabe, R. Stephan, and M. Aredes, “New concepts of instantaneous active and reactive powers in electrical systems with generic loads,” *IEEE Transactions on Power Delivery*, vol. 8, no. 2, pp. 697–703, 1993.

[15] M. Utvić and D. Dujić, “Generalized theory on direct arm energy control in modular multilevel converters,” *CPSS Transactions on Power Electronics and Applications*, vol. 5, no. 4, pp. 388–399, 2020.